Title
The Cryogenic Mechanical Properties of Vintage III Al-Cu-Li-Zr Alloy 2090-T81

Authors
Chu, D.
Morris, J.W.

Publication Date
1991-02-01

LBL-29395

Center for Advanced Materials

CAM

Presented at the Metallurgical Society Annual Meeting,
New Orleans, LA, February 18–21, 1991

The Cryogenic Mechanical Properties of Vintage III Al-Cu-Li-Zr Alloy 2090-T81

D. Chu and J.W. Morris, Jr.

February 1991

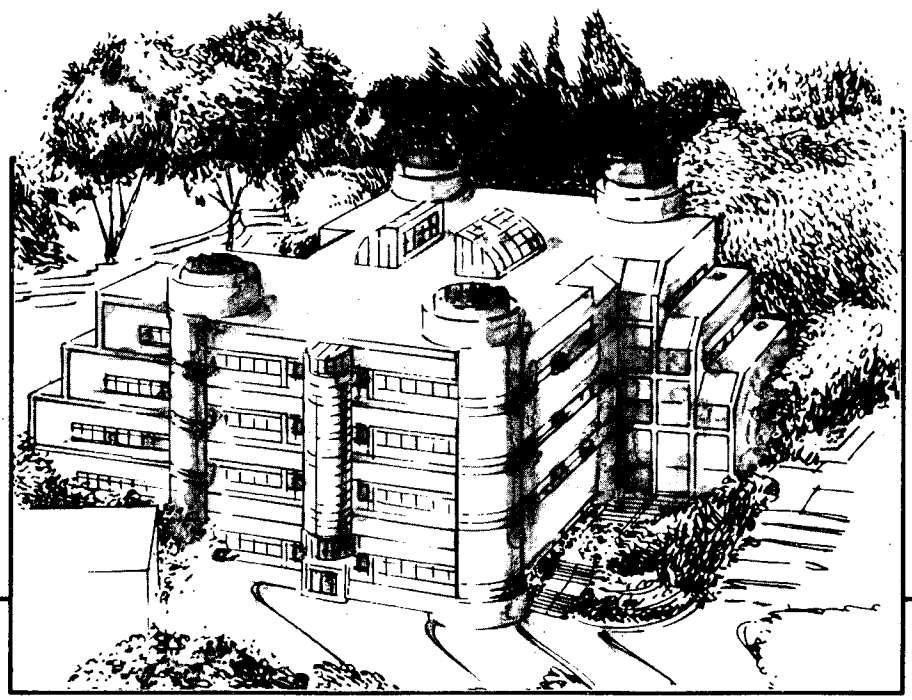

Materials and Chemical Sciences Division

Lawrence Berkeley Laboratory • University of California

ONE CYCLOTRON ROAD, BERKELEY, CA 94720 • (415) 486-4755

Prepared for the U.S. Department of Energy under Contract DE-AC03-76SF00098

DISCLAIMER

LBL 29395

The Cryogenic Mechanical Properties of Vintage III Al-Cu-Li-Zr Alloy 2090-T81

David Chu and J.W. Morris, Jr.

Center for Advanced Materials
Materials and Chemical Sciences Division
Lawrence Berkeley Laboratory
1 Cyclotron Road
Berkeley, CA 94720

and

Department of Materials Science and Mineral Engineering
University of California

February 1991

This work was supported by the Director, Office of Energy Research, Office of Basic Energy Science, Materials Sciences Division of the U.S. Deparment of Energy under Contract No. *DE-AC03-76SF00098.*

The Cryogenic Mechanical Properties of Vintage III Al-Cu-Li-Zr Alloy 2090-T81

David Chu and J.W. Morris, Jr.

Center for Advanced Materials, Lawrence Berkeley Laboratory and
Department of Materials Science and Mineral Engineering, University of California
Berkeley, CA 94720

The cryogenic mechanical properties of a 12.7 mm (0.5 in.) Vintage III 2090-T81 (Al-3.05Cu-2.16Li-0.11Zr in weight percent) plate material are studied. The results indicate that the through-thickness and in-plane anisotropies in the yield strength of Vintage I 2090-T81 are reduced in the Vintage III material by utilizing a partial recrystallization step during the thermomechanical processing, but at some cost to the elongation and cryogenic fracture toughness. Sharp discontinuities in the microstructure resulting from this thermomechanical treatment give rise to distinct differences in the mechanical behavior between those regions that undergo recrystallization and those that do not. The reduced ductility observed in Vintage III 2090-T81 relative to Vintage I 2090-T81 is a result of an overall decrease in slip homogeneity and subsequent work hardening ability, while the reduced cryogenic toughness is due in part to the disruption of the monolithic unrecrystallized grain structure previously observed in Vintage I 2090-T81. A comparative study between the microstructural and mechanical properties of the two vintages of 2090 indicates that a fully unrecrystallized structure is essential for excellent cryogenic toughness.

Introduction

Aluminum based alloys containing lithium are attractive structural materials due to their low density and high stiffness and strength relative to current high strength aluminum alloys.[1,2] Applications for these alloys were realized early in the aircraft industry where design studies have shown that reductions in weight density provide the most efficient means of increasing both weight savings and aircraft performance.[3,4,5] In general, a 3% reduction in density and a 5 to 6% increase in the modulus are associated with each weight percent addition of lithium.[6,7] As part of a continuing effort to develop these alloys, an aluminum-copper-lithium alloy designated 2090 was introduced by the Aluminum Company of America (Alcoa).[8] More recent work has shown that 2090 has an excellent combination of strength and toughness at cryogenic temperatures.[9-14] As a result, 2090-T81 and alternative aluminum-lithium alloys are projected to replace the aluminum alloy 2219-T87 that is currently used in cryogenic applications.[10,15] Several investigations are presently underway to assess the use of 2090 as a structural material for both aircraft and aerospace systems;[6] in particular, for applications such as fuselage skins, stringers, frames, and welded cryogenic tankage.[6,16]

Despite its initial promise, studies on 2090-T81 have revealed a number of problems. The one which has received the most critical attention is yield strength anisotropy.[17-20] This problem is directly related to the particular thermomechanical treatment used to produce the final product. The process is a proprietary one that includes a thermomechanical reduction into plate form, a solution heat treatment, a subsequent 6 to 8% stretch, and a final peak-age at 163°C for approximately 24 hours.[15] Initially designed to produce a high strength, fully unrecrystallized microstructure, the process results in a material which is highly textured and contains highly elongated grains.[8,9,12-15]

The yield strength of the first production 2090-T81 12.7 mm (0.5 in.) plate material (Vintage I) follows a parabolic profile through the thickness of the sheet with a maximum value near mid-thickness.[8,17,18,20,21] Differences of approximately 120 MPa (17 ksi) between tensile samples tested at mid-thickness and tenth-thickness have been reported.[8] In addition, drops of over 70 MPa (10 ksi) have been reported for off-axis tensile loadings.[8,16,19-21] Both anisotropies have been linked to the hot-rolled texture induced by rolling during processing. Specifically, the distribution and presence of the strengthening phase T_1 (Al_2CuLi) has been shown to play the dominant role in the through-thickness and in-plane yield strength variations.[17,18,19] Other microstructural features including grain shape, lithium and copper in solid solution, and non-uniform quench rates are also cited as possible mechanisms.[17]

In response to these problems of anisotropy, Alcoa introduced a modification of the alloy 2090 that is referred to as Vintage III 2090-T81.[20,21] This new vintage is projected to reduce the yield strength anisotropy associated with the earlier vintage. This paper concentrates on the microstructural and mechanical properties of Vintage III 2090-T81 and how they compare with those obtained from Vintage I 2090-T81.

Experimental Procedure

The material investigated in this study was a Vintage III 2090 plate that was provided by Alcoa in the form of a 12.7 mm (0.5 in.) plate in the -T81 condition, solution heat treated, stretched and peak-aged. This temper is also referred to as -T8E41 in earlier publications. The nominal composition ranges for 2090 in weight percent are tabulated in Table I. Actual compositions for both Vintage I[9,12,15] and Vintage III materials were determined by atomic absorption spectroscopy and are also shown in Table I.

Mechanical tests were done at four different temperatures: 300K (room temperature), 200K (dry ice and alcohol), 77K (liquid nitrogen), and 4K (liquid helium). To characterize the through-thickness anisotropy of the material, tensile test specimens were cut parallel to the rolling direction (longitudinal) at five levels as illustrated in Figure 1: mid-thickness (T/2), quarter-thickness, top and bottom (T/4 and 3T/4), and tenth-thickness, top and bottom (T/10 and 9T/10). Flat tensile specimens were opted for so that the various microstructures through the plate thickness could be isolated and tested individually. Characterization of the in-plane anisotropy was accomplished by extending the test matrix to include additional off-axis tensile test specimens: 45° from the rolling

Element	2090 (composition range)	Vintage III 2090-T81*	Vintage I 2090-T81*
Al	bal	bal	bal
Cu	2.4-3.0	3.05	2.86
Li	1.9-2.6	2.16	2.05
Zr	0.08-0.15	0.12	0.12
Fe	0.12	0.08	<0.02
Others	<0.05	<0.01	<0.02

* *As received.*

Table I: Compositions in Weight Percent of Aluminum-Copper-Lithium Alloy 2090-T81.

direction at each of the five levels, and perpendicular to the rolling direction (long-transverse) at mid-thickness and both quarter-thickness positions. All sides of the tensile specimen gage were polished to 600 grit prior to testing to minimize any effect from notch sensitivity.

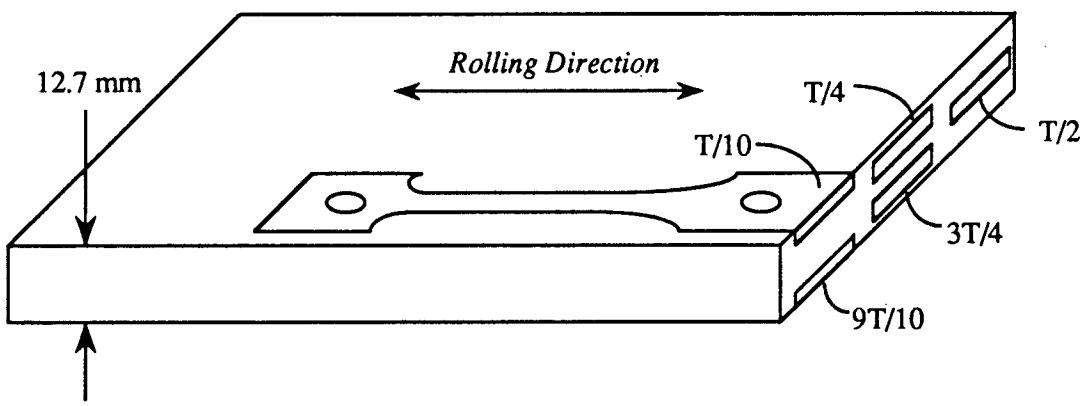

Figure 1: Schematic illustration showing the position of the through-thickness tensile specimens relative to the original plate material.

All tensile tests were conducted in displacement control. Displacement rates corresponded to strain rates of approximately 2.5×10^{-4} per second within the plastic range. Engineering stress and strain data were collected via computer and reduced prior to further computation. The data were then converted to true stress (σ) and strain (ε) values. The instantaneous strain hardening rate, $\partial\sigma/\partial\varepsilon$, was calculated by means of a sliding five-point fit to the parabolic relation $\sigma = A\varepsilon^n$, where A is the stress at unit strain and n is the strain hardening exponent which varies with the amount of deformation.[22,23] The analysis of the

tensile tests includes comparisons of the values of true stress, true strain, and strain hardening rate and their relationships to one another under the various test conditions. Strain hardening curves are presented in two forms: as a function of true stress and true strain.

Overlay plots of the true stress, σ, and strain hardening rate, $\partial\sigma/\partial\varepsilon$, as a function of the true strain, ε, illustrate the stability of plastic deformation and the relative ductility at failure. Such plots were used by Glazer, et al.[12,15] to study the macroscopic tensile behavior of 2090 and 2091. Geometric instability in tension occurs when the strain hardening rate equals the true stress ($\partial\sigma/\partial\varepsilon = \sigma$).[24] Upon the satisfaction of this relation, the increase in stress due to the decrease in cross-sectional area exceeds that due to work hardening. Deformation is then no longer stable, and necking begins. The difference, $\partial\sigma/\partial\varepsilon - \sigma$, is a measure of the instantaneous stability of plastic deformation. The value of the difference at failure can be used to distinguish between cases of premature or brittle fracture ($\partial\sigma/\partial\varepsilon > \sigma$) and failure due to the macroscopic geometric instability ($\partial\sigma/\partial\varepsilon \leq \sigma$).

Since strain is a not a thermodynamic variable and cannot be used to describe the state of a given material, it is common to plot the work hardening rate, $\partial\sigma/\partial\varepsilon$, versus the true stress, σ, rather than the true strain, ε. Basic theories relate the product $\sigma(\partial\sigma/\partial\varepsilon)$ to the inverse of the dislocation mean free path and the true stress, σ, to the dislocation density.[25] Such plots are utilized to separate and identify the effect of temperature on the microscopic development of work hardening for tensile specimens under various testing conditions. Plots of this form, shown in Figure 2, exhibit a line of zero slope in the idealized case, where the increase in dislocation density is compensated by a corresponding decrease in the dislocation mean free path. In this study, the line of zero slope is referred to as the region of stable deformation and is defined by the two bordering inflections. Deviations from this plateau represent increased localization of slip within the material.

The fracture toughness of the Vintage III 2090-T81 plate was measured by determining K_{Ic} values from measured J_{Ic} values for standard 12.7 mm (0.5 in.) thick compact tension specimens with W = 50.8 mm (2.0 in.) according to the single specimen compliance technique in the 1987 ASTM Standard E813. Tests were conducted for three orientations (L-T, T-L, L-45°), each at three different test temperatures (300K, 77K, 4K). Fracture surfaces were examined by scanning electron microscopy.

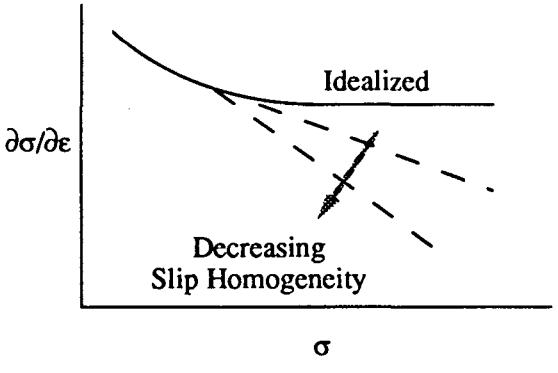

Figure 2: Schematic illustration of the idealized work hardening behavior as a function of true stress σ for polycrystals shown in bold (After Mecking, ref. 25). Dotted line shows the conceptual deviation from zero slope of the region of stable deformation resulting from a decrease in deformation homogeneity.

Results & Discussion

Microstructure

Early optical work revealed a larger grain size associated with the more recent vintage. In addition, the grain size was found to vary considerably with through-thickness plate position. The grains in the earlier vintage are highly elongated with a mean grain size of approximately 2000 x 400 x 25 μm throughout the material.[15] In contrast, the grain size in Vintage III 2090-T81 ranges from approximately 3500 x 800 x 50 μm at mid-thickness to as great as 10000 x 800 x 300 μm at quarter-thickness.[26]

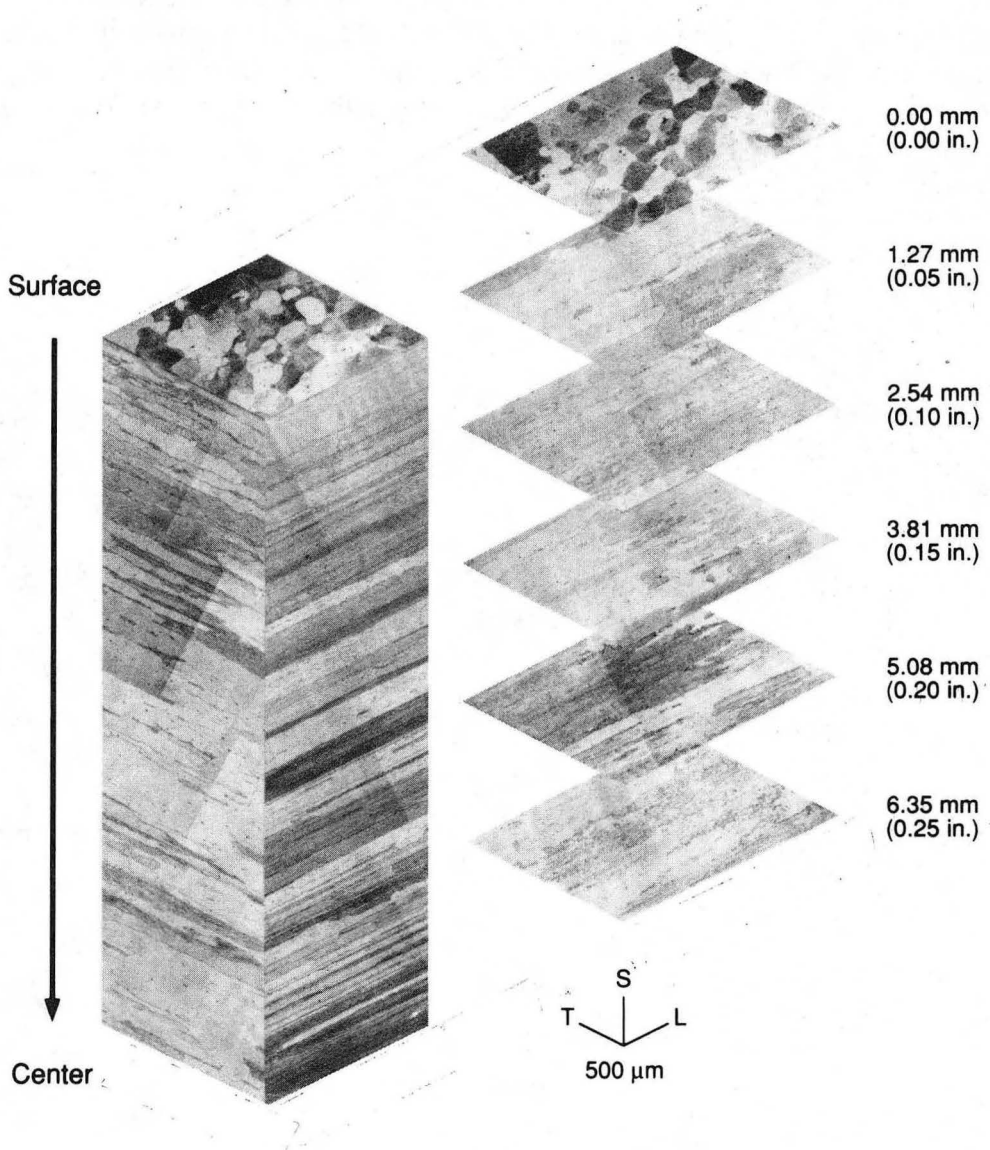

Figure 3: Optical micrograph showing the microstructure from the top surface to mid-thickness of Vintage III 2090-T81. (XBB 902-882)

A through-thickness optical survey incorporating the top portion of the plate material (surface to mid-thickness), shown in Figure 3, reveals that the wide range of grain sizes is also accompanied by a wide range of grain morphologies. Relatively thin grains with a healthy distribution of subgrains are found at mid-thickness of the plate whereas a region consisting of much larger grains with very few subgrain features is observed near quarter-thickness. The transition between the two grain morphologies is abrupt as highlighted in Figure 4. The discrete change suggests that the material was partially recrystallized at some point during the thermomechanical processing where the thinner grains are those which remain unrecrystallized while the thicker grains are recrystallized grains which undergo further rolling. Bull and Lloyd[27] have noted a similar structure in aluminum-lithium alloys undergoing low overaging temperatures. Toward the surface, a slight decrease in grain size and a return of subgrain features are noted. In contrast to the elongated grains expected in a hot-rolled material, an approximately 500 μm thick layer of equiaxed grains with varying diameters of 500 to 1000 μm are found at the surface. The increased contrast obtained from these grains relative to the rest of the plate suggests that this equiaxed layer may be the result of surface recrystallization upon the final solution heat treatment.[28]

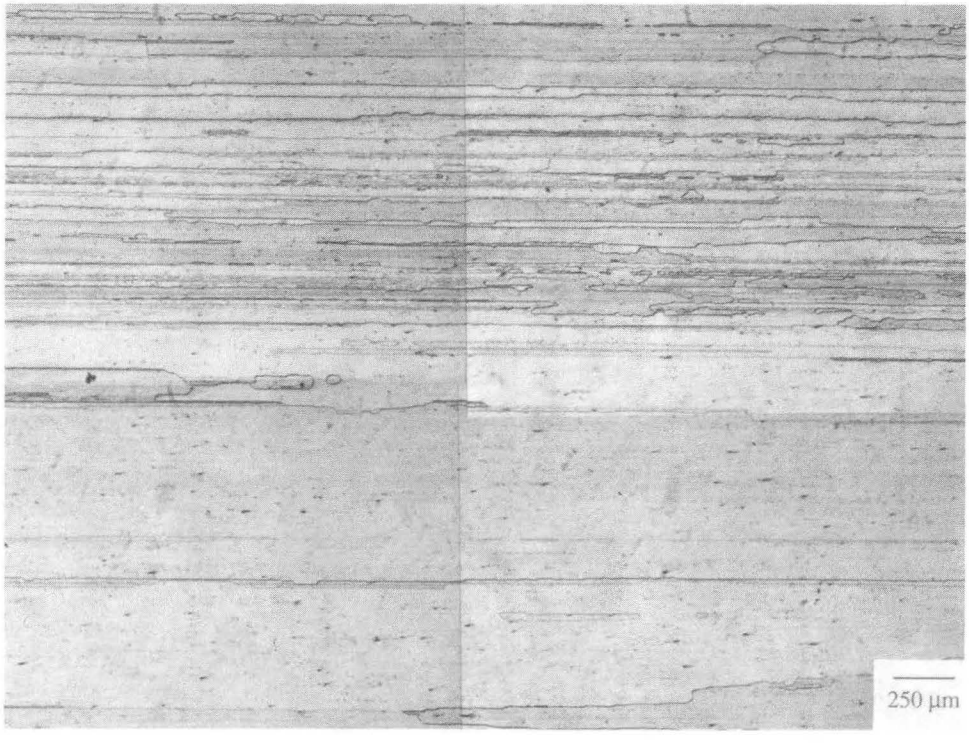

Figure 4: Optical micrograph showing the boundary between relatively thin grains near mid-thickness and thicker grains below. (XBB 906-5007)

The dramatic microstructural variations observed, such as the sharp boundary between the regions of fully unrecrystallized and pre-recrystallized microstructures (Figure 4), suggest an equally strong variation in the subsequent mechanical properties. In general, the principal difference between unrecrystallized and recrystallized structures resides in the degree of grain boundary misorientation.[29] Recrystallization softens the intense texture developed within rolled aluminum alloy products. Although an increase in isotropy in the plane is achieved, the subsequent side effect is the increase in grain boundary misorientation which leads to intergranular fracture and lower fracture toughness when the grain size is large.[30,31] This behavior becomes more notable at cryogenic temperatures, as evidenced by the low fracture toughness of recrystallized aluminum-lithium alloys.[15,16] Unrecrystallized structures, such as Vintage I 2090-T81, alleviate this stress concentration by reducing the degree of grain misorientation and thus accommodating slip continuity across grain boundaries.[29] These structures increase the probability of higher energy transgranular fracture and improve cryogenic toughness. However, the directionality associated with unrecrystallized structures results in improvement only in one orientation, namely parallel to the rolling direction. As will be shown below, these factors create a dependency of the mechanical behavior of Vintage III 2090-T81 on the through-thickness position.

Despite the wide range of microstructures observed, earlier TEM work revealed no differences in the distribution of the strengthening precipitates, δ' and T_1 at various through-thickness positions.[26] Additionally, no embrittling δ precipitate phase was observed in the bright field images of selected samples. Thorne et al.[32] have reported a lithium depletion zone induced by the surface recrystallization discussed above. However, TEM investigations at the surface revealed no significant decrease in the volume fraction of δ' or T_1.[26]

Tensile Properties

For the majority of Vintage III 2090-T81 tensile specimens, the reduction in the cross-sectional area was minimal. A few exceptions to this trend occurred for tensile specimens taken at 3T/4 and 9T/10 where the combination of intergranular delamination and partial fracture produced large area reductions within the material still intact and, subsequently, exaggerated total elongations. Uniform elongations were unperturbed by this behavior and remained valid parameters for comparison. A number of the more prominent results are highlighted and discussed below.

Figure 5a shows that the longitudinal yield strength anisotropy through the thickness of Vintage I 2090-T81 12.7 mm (0.5 in.) plate is reduced in the Vintage III material. Unlike the monotonic drop in yield strength observed from mid-thickness to the surface in the earlier vintage, Vintage III 2090 exhibits a minimum near both quarter-thickness positions bordered by maxima at mid-thickness and the two surfaces. The result is a strength variation of no more than approximately 100 MPa (15 ksi) at room temperature in the longitudinal yield strength, a 15% reduction in the 120 MPa (17 ksi) difference of the earlier vintage. Corresponding plots for 45° and long-transverse specimens exhibit similar trends to that shown in Figure 5a although at lower levels and to lesser degrees.

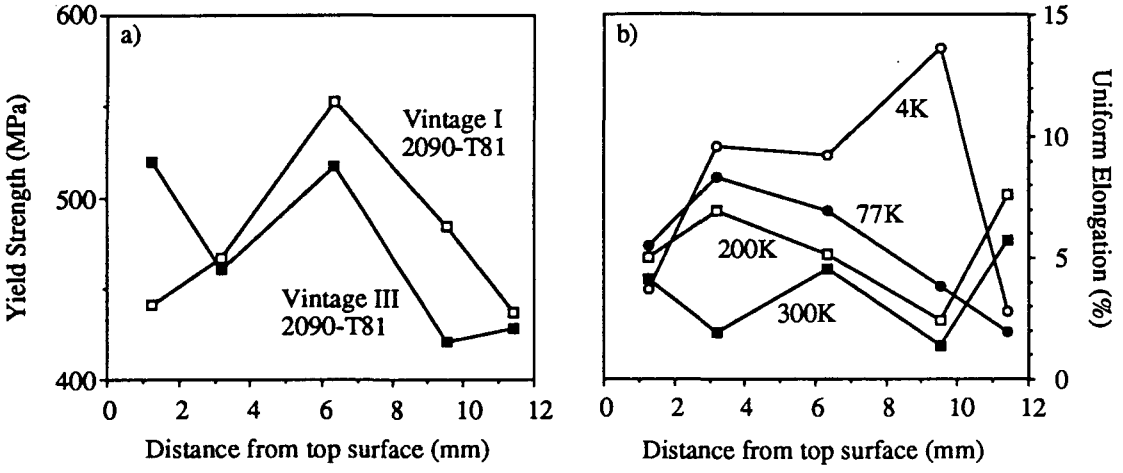

Figure 5: a) Variation of the yield strength as a function of the through-thickness position for Vintage I and Vintage III 2090-T81 longitudinal tensile specimens tested at 300K. b) Variation of the uniform elongation with through-thickness position for Vintage III 2090-T81 longitudinal tensile specimens.

Room temperature uniform elongation values for longitudinal specimens exhibit similar trends as their corresponding yield strengths. However, this profile varies dramatically with decreasing temperature, as depicted in Figure 5b. Additionally, an asymmetry of mechanical properties can also be noted. T/4 specimens exhibit a large jump in uniform elongation between 300K and 200K, whereas a similar jump does not occur for 3T/4 specimens until lower temperatures.

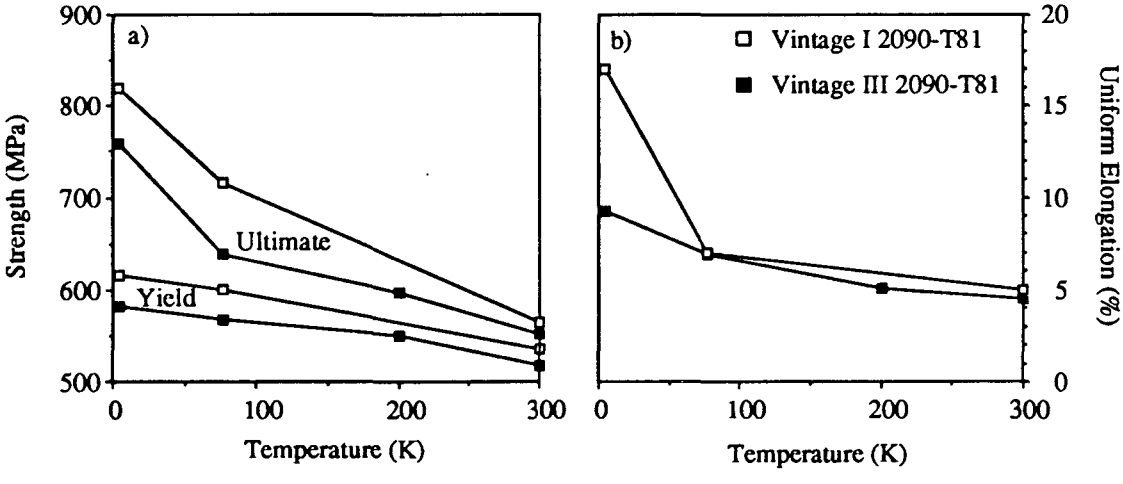

Figure 6: Comparison of the a) yield and ultimate strengths, and b) uniform elongation as a function of temperature for Vintage I and Vintage III 2090-T81 longitudinal tensile specimens taken at mid-thickness.

A plot of the data obtained from longitudinal tensile specimens at mid-thickness reveals an increase in strength and uniform elongation values with decreasing temperature. This trend is similar to what is observed for the earlier vintage, as shown in Figure 6. Although the level of the temperature induced strength increase is lower for the Vintage III material, the degree of the strength increase is similar. The improvement trend of the uniform elongation measured for Vintage III 2090-T81 at mid-thickness parallels that exhibited by its predecessor, except at 4K where Vintage I 2090 exhibits roughly twice the elongation of Vintage III 2090. The dual drop in both strength and elongation observed in the Vintage III material relative to the Vintage I material is unusual; an inverse relation between the two is more common. The increases in strength values with decreasing temperature are observed for all through-thickness positions and orientations similar to those shown in Figure 6a. However, only longitudinal uniform elongations taken at quarter-thickness mimic this trend. Both T/10 and 9T/10 longitudinal specimens and all 45° specimens exhibit a drop in the uniform elongation between 200K and 77K. Fracture surface analysis has shown both of these anomalies to be a consequence of an intruding fracture mode change.

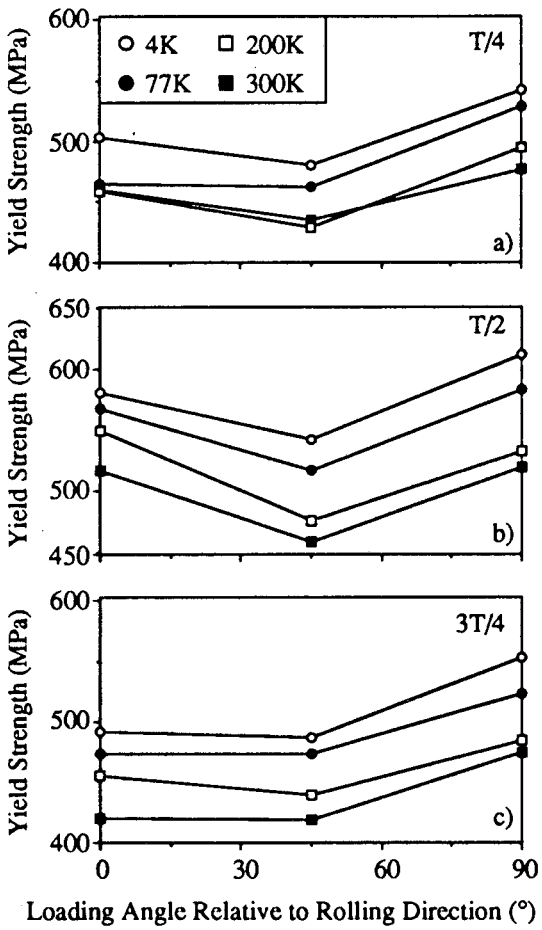

Figure 7: Variation of the yield strength with orientation for Vintage III 2090-T81 tensile specimens taken at a) T/4, b) T/2, c) 3T/4.

In order to examine the issue of in-plane anisotropy, the yield strengths compiled in Table II can be replotted as a function of testing orientation, as illustrated in Figure 7. With few exceptions, the results show a consistent drop in strength at 45° at all levels of the material. The magnitude of this drop, however, varies with each through-thickness position. Mid-thickness tensile samples reveal the most dramatic drop, ranging from 35 MPa (5 ksi) to 70 MPa (10 ksi) between longitudinal and 45° orientations, respectively. In contrast, quarter-thickness specimens do not drop by more than 25 MPa (3.5 ksi) for all test temperatures. Figure 8 replots the through-thickness position dependency of the in-plane anisotropy at room temperature. Compared to Vintage I 2090-T81, quarter-thickness specimens exhibit a substantial reduction of the in-plane anisotropy. Mid-thickness specimens, however, reveal little change.

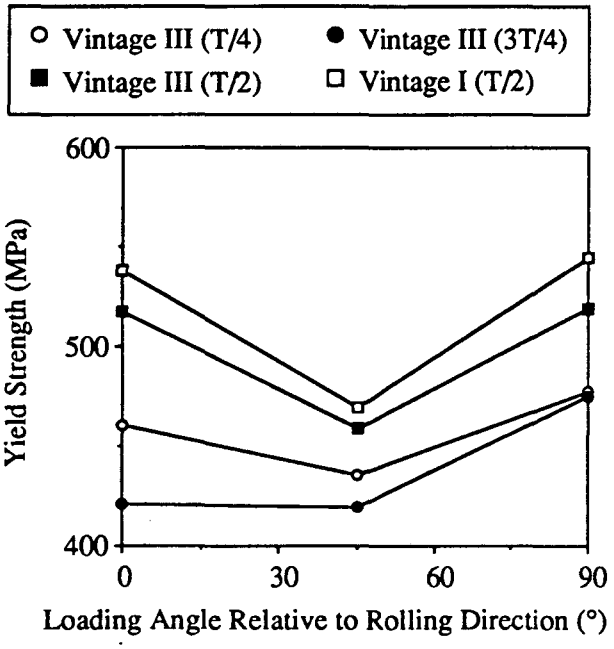

Figure 8: Comparison of the yield strength as a function of the in-plane orientation for Vintage I 2090-T81 tensile specimens taken at mid-thickness and Vintage III 2090-T81 tensile specimens taken at mid-thickness and quarter-thickness.

Fracture Properties

A plot summarizing the calculated K_{Ic} values obtained for Vintage III 2090-T81 is shown in Figure 9. The fracture toughness shows an improvement between 77K and 4K for L-T and T-L oriented specimens while L-45° K_{Ic} values exhibit a slight drop in toughness. The anomalous drop in the measured fracture toughness between 77K and 4K exhibited by the L-45° specimens is coincident with the equally anomalous drop in the 45° tensile elongation value at 77K; the maximum L-45° K_{Ic} value, which occurs at 77K, coincides with the minimum 45° uniform elongation value. As mentioned above, this drop is due to a change in the fracture mode occurring for off-axis tests.

Figure 9: Variation of the plane strain fracture toughness with temperature for Vintage III 2090-T81 L-T, L-45°, T-L J_{Ic} specimens. Values obtained for Vintage I 2090-T81 L-T J_{Ic} specimens are shown for comparison.

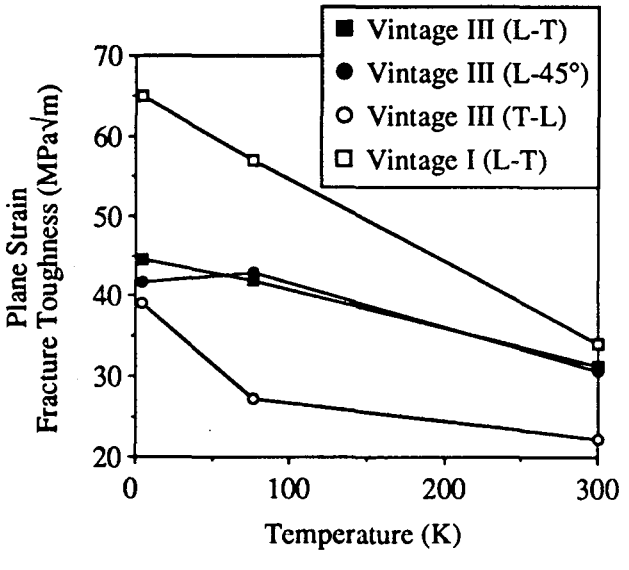

It is important to recall that establishing relationships between tensile and fracture properties are made increasingly difficult by the extent of the through-thickness anisotropy. Unlike the tensile properties, which can be measured for a given position in the thickness, fracture properties incorporate the entire thickness of the plate. As a result, measured toughness values are not only a result of the interplay between the intergranular and intragranular microstructures, but also of the state of stress throughout the material.

A plot comparing the strength and toughness of Vintage III 2090-T81 along with 7075-T6, Vintage I 2090-T81, 2219-T87,[8,15,20,21] and the set of aerospace aluminum alloys at room temperature is shown in Figure 10. Although Vintage III 2090-T81 does not fare well compared to its predecessor at cryogenic temperatures, its toughness is still superior to 7075-T6, the alloy 2090 was originally designed to replace.

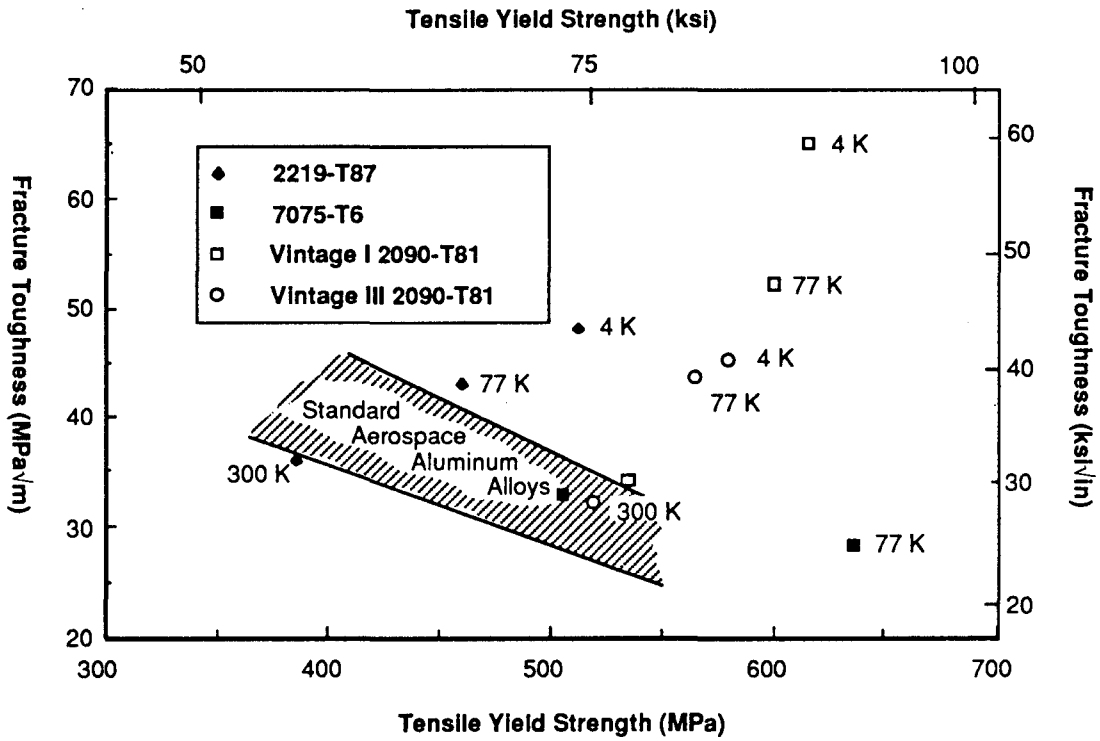

Figure 10: The strength-toughness-temperature relationship of the aluminum alloys 7075-T6, 2219-T87, Vintage I 2090-T81, and Vintage III 2090-T81. The strength-toughness trend line for advanced aerospace aluminum alloys at room temperature is also shown for comparison.

Tensile Behavior

Overlay plots of both $\partial\sigma/\partial\varepsilon$ and σ versus ε obtained from longitudinal tensile specimens taken at mid-thickness for all four test temperatures are shown in Figure 11. In all cases, failure occurs when the true stress is approximately equal to the instantaneous

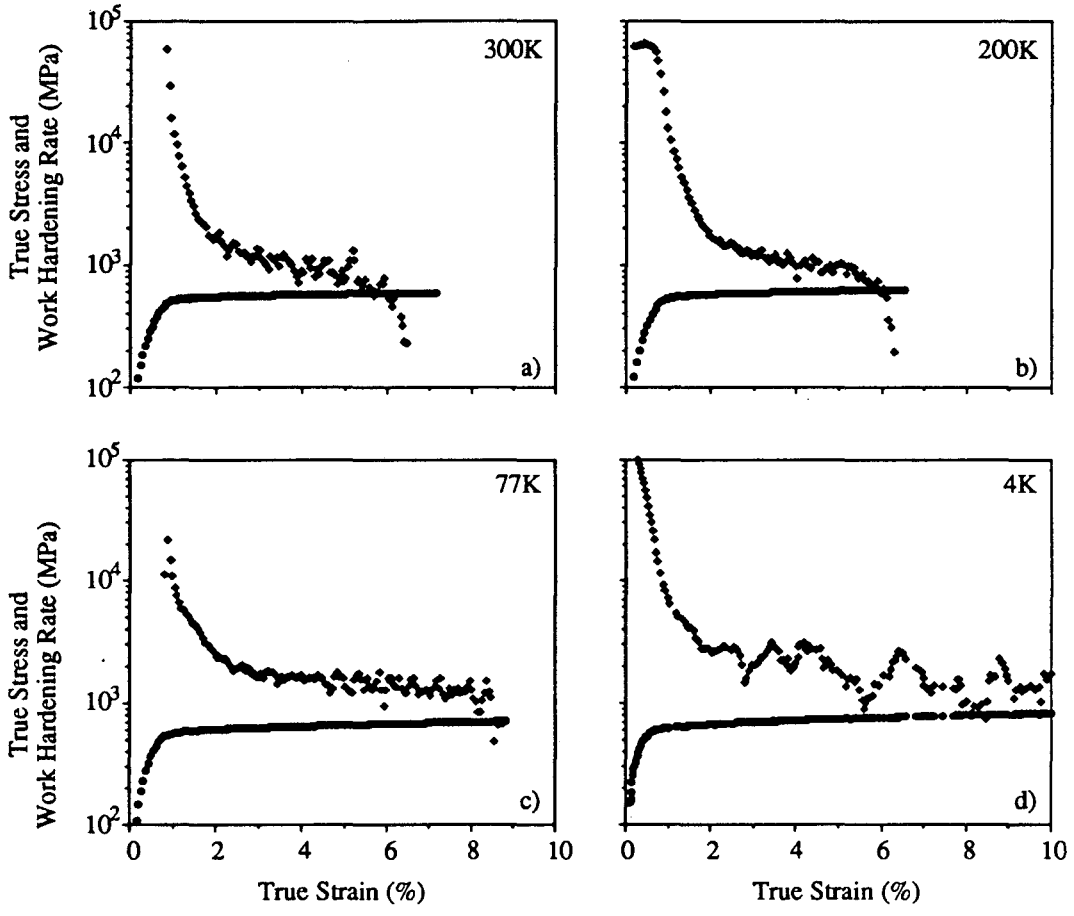

Figure 11: Comparison of the true stress and work hardening rate as a function of true strain for Vintage III 2090-T81 longitudinal tensile specimens taken at mid-thickness and tested at a) 300K, b) 200K, c) 77K, and d) 4K.

work hardening rate. Despite the fact that the intersection of σ and $\partial\sigma/\partial\varepsilon$ are well delineated at 300K and 200K only, it is clear that failure in tension occurs near the point of geometric instability and is not due to a premature brittle fracture. A comparison of the work hardening curves shows an increase of the work hardening rate with decreasing temperature (Figure 12). This increase in the work hardening level retards the onset of geometric instability and results in improved measured uniform elongation values at lower temperatures. These trends are similar to those observed for Vintage I 2090-T81 and have been linked with increased stable deformation prior to fracture at low temperatures.[12,15]

Plots of $\partial\sigma/\partial\varepsilon$ versus σ shown in Figure 13a confirm the data above, indicating that both the stress and work hardening rate at the beginning of the region of stable deformation increase with decreasing temperature. These trends are consistent with studies on Vintage I 2090-T81.[15] Kocks[30] has linked this increase in work hardening with the increasing stress required to produce deformation, since thermally activated slip processes, such as cross-slip and dislocation climb, are not operative at lower temperatures. The increase in work

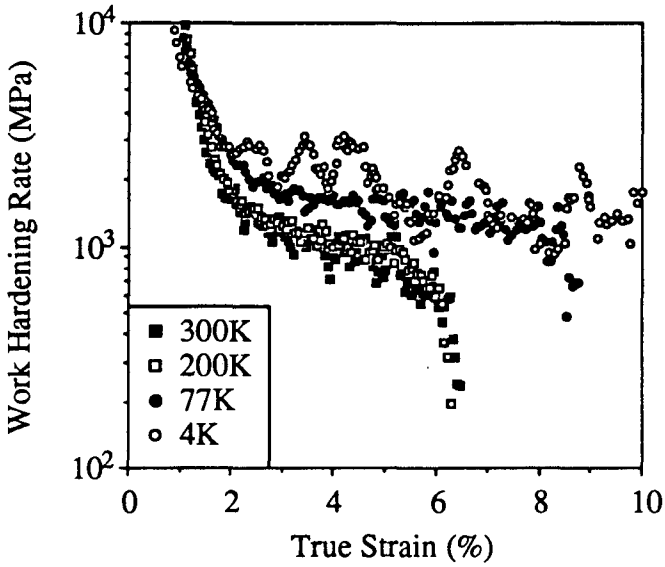

Figure 12:
Temperature variation of the work hardening rate as a function of true strain for Vintage III 2090-T81 longitudinal tensile specimens taken at mid-thickness.

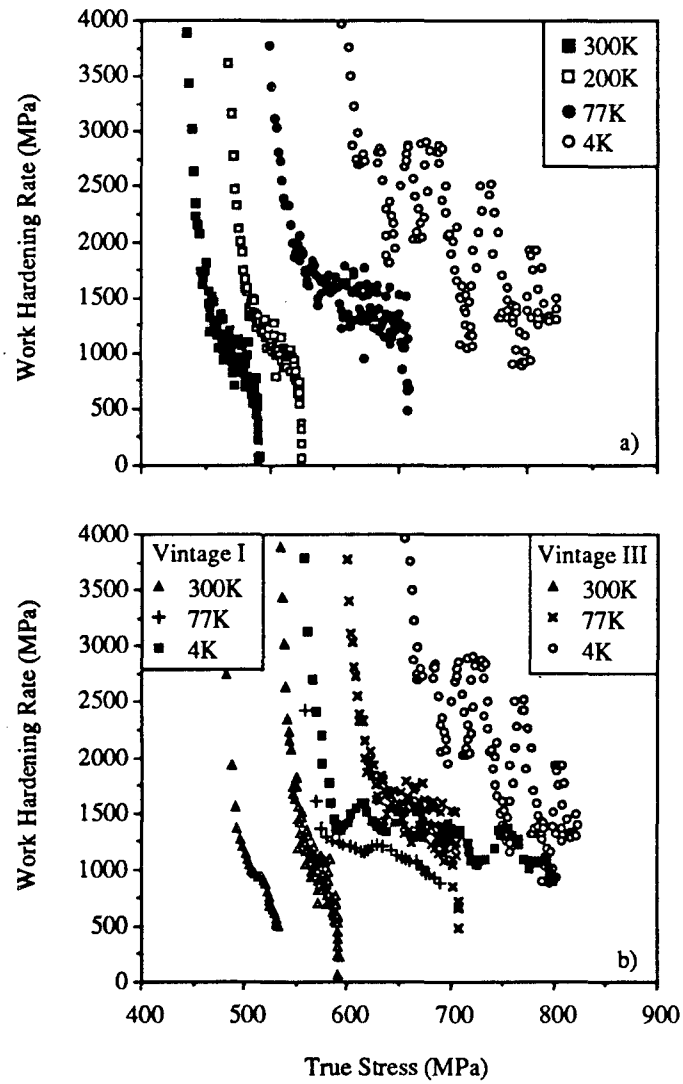

Figure 13:
a) Temperature variation of the work hardening rate as a function of true stress for Vintage III 2090-T81 longitudinal tensile specimens taken at mid-thickness. b) Same data replotted with Vintage I 2090-T81 longitudinal tensile specimens taken at quarter-thickness (After Glazer, ref. 15) for comparison.

hardening with decreasing temperature is accompanied by an increase in slip homogeneity as evidenced in Figure 13a by the approach to zero slope of the region of stable deformation. However, a comparison of the strain hardening behavior of the two vintages (Figure 13b) shows that the region of stable deformation for Vintage III 2090-T81 initiates at a higher value of the work hardening rate for all temperatures, differing by as much as 1500 MPa at 4K. The region of stable deformation for Vintage III 2090-T81 also decreases at a more rapid pace than its predecessor. These two factors combined indicate that Vintage III 2090 exploits its work hardening ability earlier in the course of the tensile test relative to Vintage I 2090-T81. The rapid decrease in this work hardening may then be due to the inability of subsequent hardening to overcome the inherent softening mechanisms of the material. At 300K this effect is less obvious.

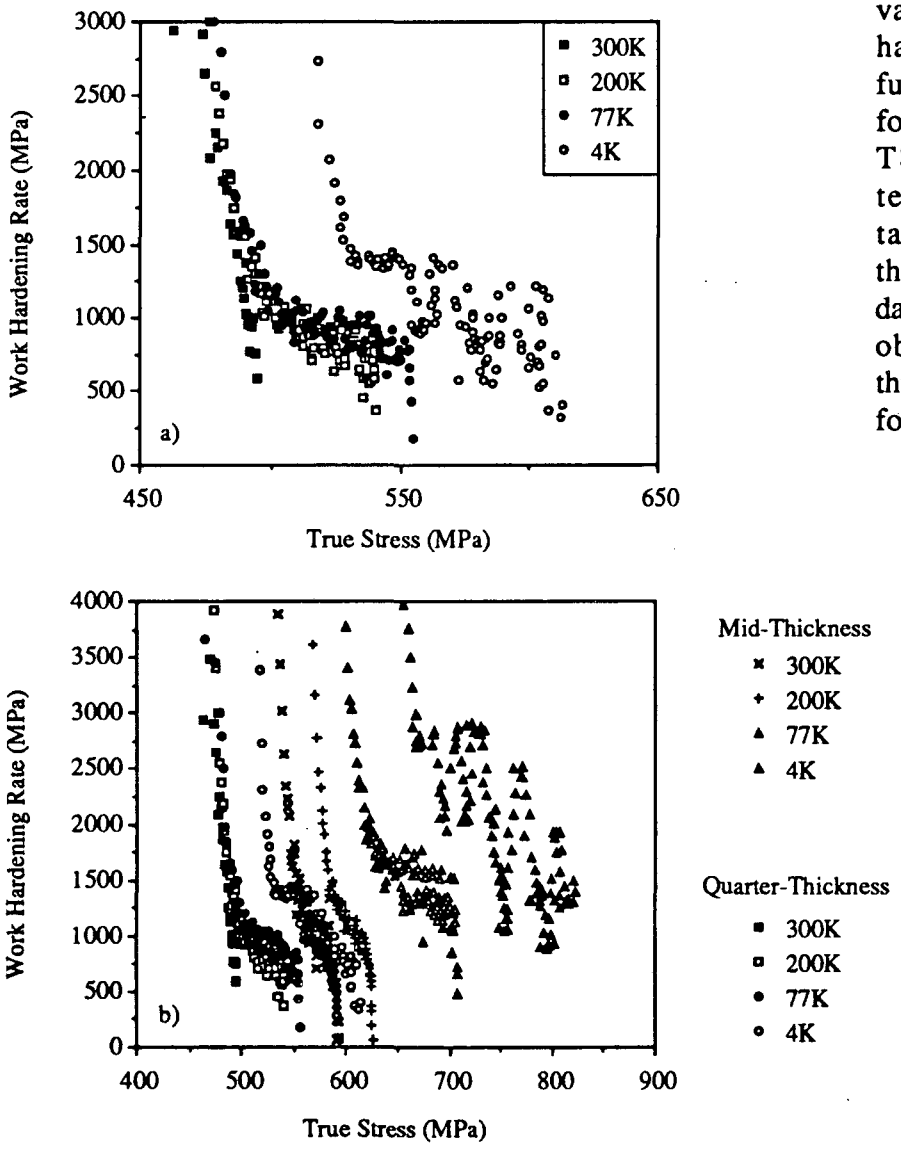

Figure 14: a) Temperature variation of the work hardening rate as a function of true stress for Vintage III 2090-T81 longitudinal tensile specimens taken at quarter-thickness. b) Same data replotted with that obtained from mid-thickness (Figure 13a) for comparison.

Similar to mid-thickness tensile specimens, failure of quarter-thickness tensile specimens occurs at approximately the instability point at all test temperatures. This behavior can be seen in Figure 14a where all four curves drop below 500 MPa before final failure. Unlike the steady increase in the work hardening rate observed at mid-thickness (Figure 12), the work hardening rate at quarter-thickness exhibits a stall between 200K and 77K. A comparison between mid-thickness and quarter-thickness specimens shows that the work hardening rate for quarter-thickness specimens is notably lower at all test temperatures, as indicated in Figure 14b. A simultaneous decrease in the yield and ultimate strengths relative to mid-thickness strengths results in quarter-thickness uniform elongations similar in value to mid-thickness specimens at 200K and 77K. The disproportionate jump in the work hardening rate at 4K relative to the corresponding strength increase at quarter-thickness then results in a superior uniform elongation. At 300K the low elongation values measured result from the absence of a region of stable deformation.

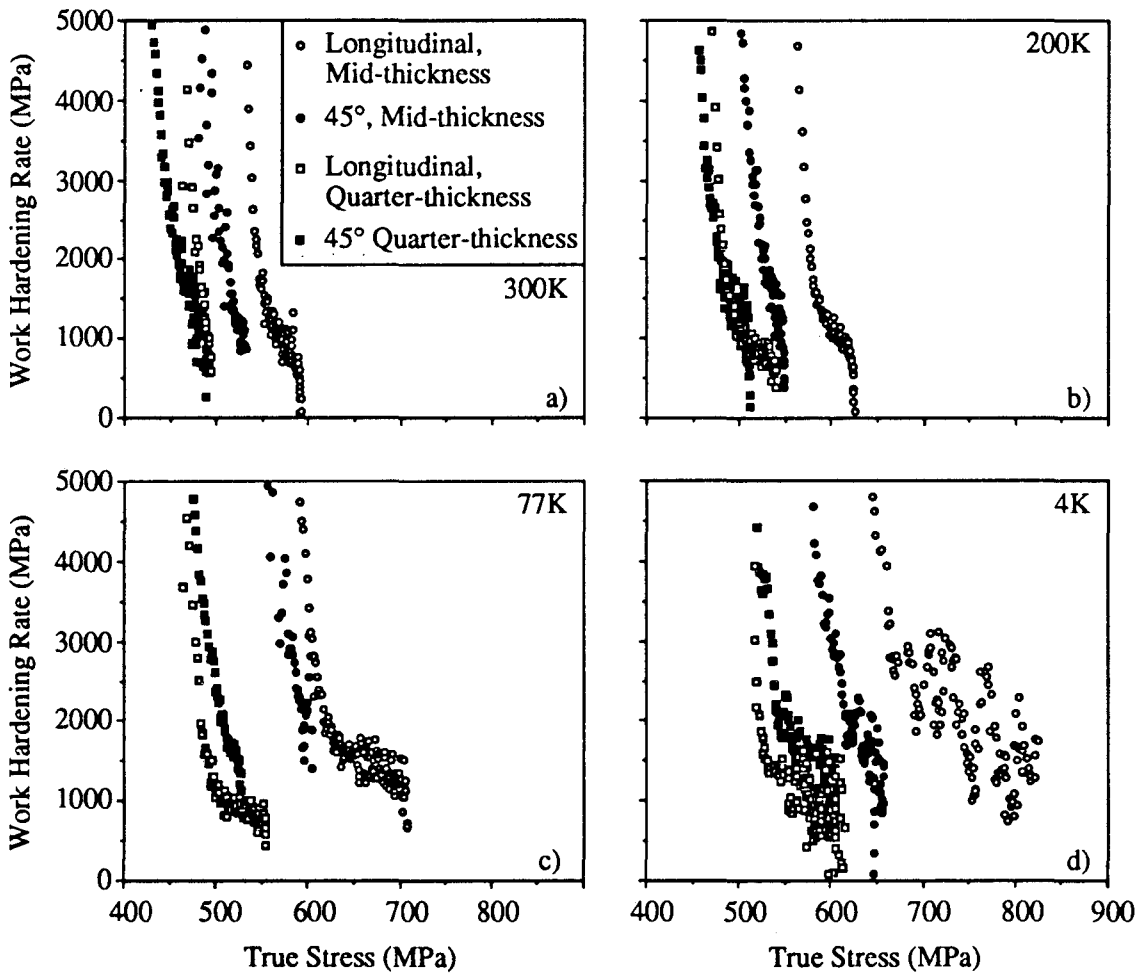

Figure 15: Comparison of the work hardening rate as a function of true stress for Vintage III 2090-T81 longitudinal and 45° tensile specimens taken at mid-thickness and at quarter-thickness and tested at a) 300K, b) 200K, c) 77K, and d) 4K.

The difference in mechanical behavior between the mid-thickness and quarter-thickness positions is best highlighted by their relative response to in-plane testing. Figure 15 illustrates the difference in the work hardening characteristic between longitudinal and 45° tensile specimens. The curves plotted for quarter-thickness tests in both orientations for the most part, lie atop of one another. In contrast, curves plotted for mid-thickness, longitudinal tests deviate from those for mid-thickness, 45° tests. In general, the separation between the two mid-thickness curves increases with decreasing temperature. As a consequence, the difference between mid-thickness and quarter-thickness tests is most dramatic at 4K. A break in the trends discussed above can be seen to occur for both mid-thickness and quarter-thickness tensile tests at 77K (Figure 15c). Although the source of this anomaly for the longitudinal tests is unknown, the break in trend for quarter-thickness tests is believed to be due to the change in the fracture mode which occurs between 200 and 77K.

Fracture Behavior

Current models for strain-controlled fracture predict proportional increases in the toughness with increases in other deformation properties, namely the yield strength, the elongation, and the work hardening rate in the absence of a fracture mode change.[33-36] Earlier work has revealed an absence of a primary fracture mode change for Vintage III L-T J_{Ic} specimens.[26] The ductile fracture mode consists primarily of transgranular shearing connected by splitting along planar grain boundaries parallel to the load axis. Previous work on Vintage I 2090-T81 have yielded similar conclusions.[12-15] Where such a preservation of fracture mode is observed, the scaling between mechanical parameters is observed.[15,37] In particular, the fracture toughness, strength, and elongation of longitudinal oriented specimens at mid-thickness and quarter-thickness all increase with decreasing temperature (Figures 6, 9, and 11). In contrast, 45° tensile tests exhibit a drop in the elongation at 77K, whereas the fracture toughness increases to a maximum. However, this break in trend is associated with a fracture mode change. When such a change in the primary fracture mode occurs in response to a change in the test temperature, it will dominate the fracture toughness response.[15,37] As such, the relation between the fracture toughness and tensile behavior based on strain-controlled fracture models are no longer stringent. The source of this fracture mode change is the subject of future work.

Vintage III 2090-T81 versus Vintage I 2090-T81

The substantial improvements in the in-plane and through-thickness anisotropies is a direct consequence of the significantly different microstructure observed for Vintage III 2090-T81. The results discussed above, both microstructural and mechanical, strongly suggest that these improvements are a result of a partial recrystallization during the thermomechanical processing. Although this partial recrystallization is effective in reducing the anisotropies associated with Vintage I 2090-T81, it creates a strong through-thickness microstructural anisotropy that may be extremely detrimental. This microstructural anisotropy separates the Vintage III 2090-T81 plate into three distinct regions: a fully unrecrystallized region surrounded by two pre-recrystallized regions. It is evident that the various polygranular microstructures observed give rise to varying degrees of strength,

toughness, and ductility. Subsequently, the improvements are highly through-thickness position dependent.

It is apparent that Vintage III 2090 attempts to mix the features of recrystallized and unrecrystallized structures. In this way, both the through-thickness and in-plane anisotropies may be lessened without loss to the cryogenic strength-toughness combination. Despite the non-ideal result, the strength-toughness combination is still superior to the current aerospace aluminum alloy 2219-T87 (Figure 10). The data accumulated in this study strongly imply that a fully and monotonic unrecrystallized grain structure as observed in Vintage I 2090-T81 is necessary to obtain excellent cryogenic fracture toughness. A similar conclusion is arrived at by Starke and Lin[31] for aluminum alloy 2020, where the poor ductility and fracture toughness are associated with a partially recrystallized structure.

The complex microstructure of Vintage III 2090-T81 can be compared to a laminated composite. As such, the mechanical properties as a whole are strongly influenced by the properties of the constituent materials, their distribution, and the interaction among them. Consequently, caution must be taken since the reduction in the thickness of the original alloy through machining will nullify the improvements in isotropy found in this vintage.

Summary and Conclusion

The mechanical properties and mechanical behavior of Vintage III 2090-T81 in the form of a 12.7 mm (0.5 in.) plate are strongly influenced by the layered laminate-like grain structure. This grain structure can be regarded on two levels: the elongated grains found throughout most of the material provides one mode of layering while the variation in the thickness of the elongated grains provide the other. The evidence summarized below indicates that this wide spectrum of microstructures is produced by a partial recrystallization during the thermomechanical processing prior to the final solution heat treatment and aging.

The yield strength through-thickness profile exhibits minima near the quarter-thickness positions with maxima at the center and near both surfaces. This variation is an improvement over the parabolic profile of the earlier vintage. Overall, the through-thickness anisotropy is reduced by 15% at room temperature. In a similar manner, improvement in the in-plane anisotropy is also observed but is restricted to certain locations in the plate thickness. This sensitivity to plate position also results from the partial recrystallization, where the in-plane anisotropy is essentially eliminated within the pre-recrystallized region at quarter-thickness. In contrast, the region of fully unrecrystallized grains at mid-thickness do not show any significant improvement over the Vintage I material in the in-plane anisotropy.

The improvements observed in the Vintage III material comes at a great loss to the cryogenic fracture toughness. However, the lower values relative to Vintage I 2090-T81, are still superior to or at least comparable to both 7075-T6, the material originally to be

replaced by 2090, and 2219-T87, the alloy projected to be replaced by 2090 in aerospace systems. It is believed that the decreased cryogenic toughness is a direct consequence of the disruption of the monolithic, fully unrecrystallized structure originally observed in Vintage I 2090-T81 which demonstrates the necessity for a fully unrecrystallized structure in order to attain superior cryogenic toughness.

Acknowledgements

This work was supported by the Director, Office of Energy Research, Office of Basic Energy Science, Material Sciences Division of the U.S. Department of Energy under Contract No. DE-AC0376SF00098. Thanks are also extended to C. Tseng for her assistance on this paper. D. Chu was supported under a National Science Foundation Graduate Fellowship for the entire period of this work.

References

1. E.S. Balmuth and R. Schmidt: *Aluminum-Lithium Alloys*, T.H. Sanders, Jr. and E.A. Starke, Jr. eds., TMS-AIME, New York, NY, 1981, pp. 69-88.

2. G.H. Narayanan, B.L. Wilson, W.E. Quist, A.L. Wingert: Technical Report D6-51411, The Boeing Company, Seattle, WA, August, 1982.

3. R.E. Lewis, D. Webster, and I.G. Palmer: Final Report, USAF Contract F33615-77-C-5186, Technical Report No. AFML-TR-78-102, July 1978.

4. I.F. Sakata: Final Report, NASA CR-165820, NASA Contract NAS1-164634, 1982.

5. J.C. Ekvall, J.E. Rhodes, G.G. Wald: *Design of Fatigue and Fracture Resistant Structures*, ASTM STP 761, American Society for Testing and Materials, 1982, pp. 328-341.

6. E.A. Starke, Jr., T.H.Sanders, Jr., and I.G. Palmer: *J. of Metals*, 1981, pp. 24-33.

7. K.K. Sankaran,and N.J. Grant: *Aluminum-Lithium Alloys*, TMS-AIME, Warrendale, PA, 1981, pp. 205-227.

8. R.J. Bucci, R.C. Malcolm, E.L. Colvin, S.J. Murtha, and R.S. James: Final Report NSWC TR 89-106, Aluminum company of America, Alcoa Center, PA, September, 1989.

9. J.Glazer, S.L. Verzasconi, E.N.C. Dalder, W. Yu, R.A. Emigh, R.O. Ritchie, and J.W. Morris, Jr.: *Adv. Cryogenic Eng.*, vol. 32, 1986, pp. 397-404.

10. J.Glazer, J.W. Morris, Jr., S.A. Kim, M.W. Aushi, and H.M. Ledbetter: *AIAA Journal*, vol. 25, pp. 1271.

11. C. Dorward, *Scripta Metall.*, vol. 20, 1986, pp. 1379-1383.

12. J. Glazer, S.L. Verzasconi, R.R. Sawtell, and J.W. Morris, Jr.: *Metall. Trans. A*, 1987, vol. 18, pp. 1695-1701.

13. K.T. Venkateswara Rao, W. Yu, and R.O. Ritchie, *Metall. Trans. A*, 1989, vol. 20, pp. 485-497.

14. K.T. Venkateswara Rao, F.H. Hayashigatani, W. Yu, and R.O. Ritchie, *Scripta Metall.*, vol. 22, 1988, pp. 93.

15. J. Glazer: Ph.D. Thesis, LBL-27607, Berkeley, CA, July 1989.

16. W.E. Quist, and G.H. Narayanan: *Treatise on Materials Science and Technology: Aluminum Alloys - Contemporary Research and Applications*, A.K. Vasudévan and R.D. Doherty, eds., vol. 31, Academic Press, Inc., SanDiego, CA, 1989, pp. 219-254.

17. A.K. Vasudévan, W.G. Fricke, Jr., R.C. Malcolm, R.J. Bucci, M.A. Przystupa, and F. Barlat: *Metall. Trans. A*, vol. 19, 1988, pp. 731-732.

18. A.K. Vasudévan, W.G. Fricke, Jr., M.A. Przystupa, and S. Panchanadeeswaran: *Eighth International Conference on Textures of Materials*, J.S. Kallend, and G. Gottstein, des., pp. 1071-1077, TMS, Warrendale, PA, 1988.

19. E.W. Kim and N.J. Lee: *Aluminum-Lithium Alloys V*, T.H. Sanders, Jr. and E.A. Starke, Jr., eds., Materials and Component Engineering Publications, Ltd., Birmingham, England, 1989, pp. 809-816.

20. R.S. James and R.J. Bucci: Lessons Learned - Aluminum-Lithium Alloy Development, ALCOA, Alcoa Technical Center, PA, 1989.

21. R.J. Rioja, B.A. Cheney, R.S. James, J.T. Staley, and J.A. Bowers: *Structure-Property Relationships in Al-Li Alloys: Plate and Sheet Products*, ALCOA, Alcoa Technical Center, PA, 1989.

22. R.W.K. Honeycombe: *The Plastic Deformation of Metals*, 2nd ed., Edward Arnold, London, England, 1984, p. 231.

23. J.E. Hatch: *Aluminum: Properties and Physical Metallurgy*, ASM, Metals Park, Ohio, 1984, p. 110.

24. R.W.K. Honeycombe: *The Plastic Deformation of Metals*, 2nd ed., Edward Arnold, London, England, 1984, p. 457.

25. H. Mecking: *Work Hardening in Tension and Fatigue*, A.W. Thompson, ed., TMS-AIME, New York, NY, 1975, pp. 67-88.

26. D. Chu and J.W. Morris, Jr.: *Metall. Trans. A*, to be published, 90-331-A.

27. M.J. Bull and D.J. Lloyd: Aluminum-Lithium Alloys III, C. Baker, P.J. Gregson, S.J. Harris, and C.J. Peel, eds., The Institute of Metals, London, England, 1986, pp. 402-410.

28. J.E. Hatch: *Aluminum: Properties and Physical Metallurgy*, ASM, Metals Park, Ohio, 1984, p. 122.

29. E.A. Starke and W.E. Quist: *AGARD Conference Proceedings No. 444 - New Light Alloys*, AGARD, Essex, England, 1989.

30. U.F. Kocks: *Trans. ASME: J. Eng. Matls. Tech.*, 1976, vol. 98 pp. 76-85.

31. E.A. Starke, Jr. and F.S. Lin: *Metall. Trans. A*, 1982, vol. 13, pp. 2259-2269.

32. N. Thorne, A. Dubus, J.M. Lang, F. Degreve, and P. Meyer: *4th International Aluminum-Lithium Conference*, G. Champier, B. Dubost, D. Miannay, and L. Sabetay, eds., Journal de Physique, 1987, vol. 48, colloque C3, pp. 521-526.

33. G.G. Garrett and J.F. Knott: *Metall. Trans. A*, 1978, vol. 9, pp. 1187-1201.

34. R.O. Ritchie and A.W. Thompson: *Metall. Trans. A*, 1985, vol. 16, pp. 233-248.

35. R.O. Ritchie, W.L. Server, and R.A. Wulaert: *Metall. Trans. A*, 1979, vol. 10, pp. 1557-1570.

36. K. Jata and E.A. Starke, Jr.: *Metall. Trans. A*, 1986, vol. 17, pp. 1011-1026.

37. J. Glazer and J.W. Morris, Jr.: *Aluminum-Lithium Alloys V*, T.H. Sanders, Jr. and E.A. Starke, Jr., eds., Materials and Component Engineering Publications, Ltd., Birmingham, England, 1989, pp. 1471-1480.

LAWRENCE BERKELEY LABORATORY
CENTER FOR ADVANCED MATERIALS
1 CYCLOTRON ROAD
BERKELEY, CALIFORNIA 94720